

1 **New insights on the physical mechanisms sustaining**  
2 **the formation of free alternate bars in rivers**

3 **Marco Redolfi<sup>1</sup>**

4 <sup>1</sup>Department of Civil, Environmental and Mechanical Engineering, University of Trento, Italy.

5 **Key Points:**

- 6 • Essential features of migrating alternate bars can be captured by neglecting the  
7 water surface deformation
- 8 • Alternate bars formation essentially depends on an imbalance between of water  
9 weight and bottom friction, which produces flow accelerations
- 10 • We derived and tested an explicit, physically-based formula for predicting the  
11 occurrence of migrating bars in rivers

---

Corresponding author: Marco Redolfi, [marco.redolfi@unitn.it](mailto:marco.redolfi@unitn.it)

## 12 Abstract

13 Free alternate bars are large-scale, downstream-migrating bedforms character-  
 14 ized by an alternate sequence of three-dimensional scour and deposition patches that  
 15 frequently develop in rivers as the result of an intrinsic instability of the erodible bed.  
 16 Theoretical models based on two-dimensional shallow water and Exner equations have  
 17 been successfully employed to capture the bar instability phenomenon, and to estimate  
 18 bar properties such as height, wavelength and migration rate. However, the mathe-  
 19 matical complexity of the problem hampered the understanding of the key physical  
 20 mechanisms that sustain the bar formation. To fill this gap, we considered a simplified  
 21 version of the equations, based on neglecting the deformation of the free surface, which  
 22 allows us to: (i) provide the first complete explanation of the bar formation mechanism  
 23 as the result of a simple bond between variations of the water weight and flow acceler-  
 24 ation; (ii) derive a simplified, physically based formula for predicting bar formation in  
 25 a river reach, depending on channel width-to-depth ratio, Shields number and relative  
 26 submergence. Comparison with an unprecedented large set of laboratory experiments  
 27 reveals that our simplified formula appropriately predicts alternate bar formation in a  
 28 wide range of conditions. Noteworthy, the hypothesis of negligible free surface effect  
 29 also implies that bars formation is fully independent of the Froude number. We show  
 30 that this intriguing property is intimately related to the three-dimensional nature of  
 31 river bars, which allows for a gentle lateral deviation of the flow without significant  
 32 deformation of the water surface.

## 33 1 Introduction

34 Alternate bars are characterized by a sequence of large scale deposition and ero-  
 35 sion patches that alternate themselves at the two sides of the channel, showing diagonal  
 36 fronts as in the example of Figure 1. The formation of alternate bars in rivers is im-  
 37 portant from an engineering perspective, as bars can affect navigability, enhance bank  
 38 erosion and interact with instream engineering structures [e.g. *Claude et al.*, 2014].  
 39 Moreover, bars formation represents a fascinating example of self-sustained morpho-  
 40 dynamic process, which that has been considered a precursor for the formation of river  
 41 meandering and braiding [e.g., *Fredsoe*, 1978], and a main driver for channel widening  
 42 [e.g. *Repetto et al.*, 2002] and for the formation of channel bifurcations [e.g. *Redolfi*  
 43 *et al.*, 2016].

44 A large number of laboratory experiments demonstrated that downstream-migrating  
 45 alternate bars tends to spontaneously form in straight channels of constant width [e.g.  
 46 *Jaeggi*, 1984; *Fujita and Muramoto*, 1982; *Ikeda*, 1984; *Lanzoni*, 2000; *Crosato et al.*,  
 47 2012; *Nelson and Morgan*, 2018; *Redolfi et al.*, 2020]. This kind of bars, often referred  
 48 to as “free alternate bars”, are frequently observed in rivers [e.g. *Jaballah et al.*, 2015;  
 49 *Rodrigues et al.*, 2015; *Adami et al.*, 2016; *Serlet et al.*, 2018; *Church and Rice*, 2009;  
 50 *Ferguson et al.*, 2011], especially in channelized, gravel-bed rivers.

51 Two- and three-dimensional mathematical models have been employed to in-  
 52 vestigate different morphodynamic characteristics of free alternate bars, including:  
 53 the effect of sediment heterogeneity [*Lanzoni and Tubino*, 1999; *Rodrigues et al.*, 2015;  
 54 *Qian et al.*, 2017; *Cordier et al.*, 2019]; the effect of flow variability *Tubino* [1991]; *Hall*  
 55 [2004]; the interaction between free and forced (or hybrid) bars [*Tubino and Seminara*,  
 56 1990; *Duró et al.*, 2016]; the effect of suspended sediment load [*Tubino et al.*, 1999;  
 57 *Federici and Seminara*, 2006; *Bertagni and Camporeale*, 2018]; the transition from al-  
 58 ternate bars to three-dimensional oblique dunes [*Colombini and Stocchino*, 2012];  
 59 the morphodynamic effect of vegetation [*Bertagni et al.*, 2018; *Jourdain et al.*, 2019;  
 60 *Caponi et al.*, 2019].

61 Mathematical modelling allowed for the identification of the essential processes  
 62 needed to reproduce the bar formation. They revealed that three-dimensional effects  
 63 such as helical motion or flow separation are of secondary importance, so that the  
 64 process of alternate bars formation can be effectively predicted by means of depth-  
 65 averaged, two-dimensional shallow water and Exner equations. Specifically, linear sta-  
 66 bility analyses [Callander, 1969; Parker, 1976; Fredsoe, 1978; Colombini et al., 1987]  
 67 demonstrated that even for a straight channel of constant width the basic, uniform-flow  
 68 solution is inherently unstable, which leads from the spontaneous formation of long,  
 69 three-dimensional bed deformations representing free alternate bars. Moreover, these  
 70 theoretical analyses provided an useful criterion to determine marginal stability con-  
 71 ditions, which are mainly controlled by the channel width-to-depth ratio. Specifically,  
 72 bars are expected to form when the width-to-depth ratio exceeds a critical threshold  
 73 that depends on other river characteristics (primary relative roughness and Shields  
 74 number).

75 Nevertheless, the mathematical complexity of the problem limited the derivation  
 76 of explicit, physically based expressions for the critical aspect ratio as a function of  
 77 the controlling parameters, as also recently highlighted by [Crosato and Mosselman,  
 78 2020]. As a consequence, application of the theory currently requires either to numer-  
 79 ically solve a dispersion relation involving complex numbers, or to rely on plots made  
 80 available by different authors, with limited possibility to explore the space of param-  
 81 eters and the effect of different transport and friction formulae. A possible alternative  
 82 is based on empirical criteria proposed in the literature [e.g., Muramoto and Fujita,  
 83 1978; Jaeggi, 1984; Yalin and Da Silva, 2001; Ahmari and Da Silva, 2011]. Despite  
 84 being originally formulated in different ways, empirical relations can be re-expressed  
 85 in terms of the threshold value of the width-to-depth ratio that needs to be exceeded  
 86 to enable the formation of bars. However, the empirical nature of these criteria makes  
 87 it difficult to extend predictions out of the set of conditions for which they are derived.  
 88 Moreover, empirical relations do not allow for isolating the effect of the individual  
 89 physical parameters, and to assimilate information that may come from site-specific  
 90 estimations of hydraulic roughness or sediment transport relations.

91 More fundamentally, the mathematical complexity highly limited the possibility  
 92 to provide a satisfactory physical explanation of the mechanism of bar instability. A  
 93 first tentative explanation was proposed by [Einstein and Shen, 1964], who suggested  
 94 that bars may form as a consequence of helical motion, possibly reinforced by the  
 95 presence of rough banks. However, subsequent models have conclusively demonstrated  
 96 that neither three-dimensional flow nor rough banks are essential for capturing the bar  
 97 instability mechanisms. More recent explanations Nelson [1990]; Tubino et al. [1999]  
 98 are given in terms of the divergence of the flow field around bars, due to a sort of  
 99 topographic steering. However, the mechanism that produces this flow field has not  
 100 been clarified. Therefore, a complete physical description of the instability process is  
 101 substantially missing.

102 In this work, we consider a simplified version of the governing equations, in order  
 103 to: (i) derive a simple, explicitly expression for predicting bar stability conditions and  
 104 validate it by means of existing laboratory experiments; (ii) provide a physically based  
 105 explanation of the bar formation mechanism.

106 The paper is organized as follows: in Section 2 we define the governing equations  
 107 and we specify the fundamental assumptions; in the Results Section 3 we introduce  
 108 the simple criterion for predicting the formation of bars, we test it against existing  
 109 laboratory data, and we provide a physical explanation of the bar formation mecha-  
 110 nism; in Section 4 we discuss model hypotheses and associated limitations. Finally,  
 111 details about the derivation of the explicit expression for the critical aspect ratio are  
 112 reported in Appendix A .



Figure 1: Example: downstream-migrating alternate bars in the Alpine Rhine River in Switzerland,  $47^{\circ}02' N$ ,  $09^{\circ}29' E$ , 02-Apr-2012. From *Google Earth, Digital Globe (2021)*. Flow is from left to right.

## 2 Mathematical formulation

### 2.1 The governing equations

We consider an infinitely-long channel, with straight, fixed banks and rectangular cross-section of width  $W$ , whose bottom is formed by cohesionless particles with representative (e.g., median) grain size  $d$ . We adopt a two-dimensional, mobile-bed, depth-averaged shallow water model [e.g., *Parker, 1976; Colombini et al., 1987; Siviglia et al., 2013*], which can be written as a nonlinear differential system of four equations in the four dependent variables  $U$ ,  $V$ ,  $D$  and  $H$  (longitudinal and transverse velocity, water depth and water surface elevation), in the independent variables  $x, y$  (planimetric coordinates) and  $t$  (time). As sketched in Figure 2, the origin of the cartesian system of reference is positioned at the right bank, and elevations are calculated with respect to a sloping plane having longitudinal gradient  $S_0$ . The depth-averaged equations that express the conservation of momentum, liquid and solid mass read:

$$U \frac{\partial U}{\partial x} + V \frac{\partial U}{\partial y} - gS_0 + g \frac{\partial H}{\partial x} + \frac{\tau_x}{\rho D} = 0, \quad (1a)$$

$$U \frac{\partial V}{\partial x} + V \frac{\partial V}{\partial y} + g \frac{\partial H}{\partial y} + \frac{\tau_y}{\rho D} = 0, \quad (1b)$$

$$\frac{\partial UD}{\partial x} + \frac{\partial VD}{\partial y} = 0, \quad (1c)$$

$$(1-p) \frac{\partial \eta}{\partial t} + \frac{\partial qs_x}{\partial x} + \frac{\partial qs_y}{\partial y} = 0, \quad (1d)$$

where  $p$  denotes the sediment porosity and  $\eta = H - D$  indicates the bed elevation.

The set of four differential equations is then completed by specifying closure relationships. Specifically, the two components of bed shear stress are estimated as follows:

$$\{\tau_x, \tau_y\} = \rho \frac{U^2}{c^2} \{\sin \gamma_q, \cos \gamma_q\}, \quad \tan(\gamma_q) = \frac{V}{U}, \quad (2)$$

where  $c(D/d)$  is the dimensionless Chézy coefficient and  $\gamma_q$  is the angle of the velocity vector  $\vec{U}$ . The components of sediment transport are expressed as:

$$\{qs_x, qs_y\} = \sqrt{g\Delta d^3} \Phi(\theta) \{\sin \gamma_s, \cos \gamma_s\}, \quad (3)$$

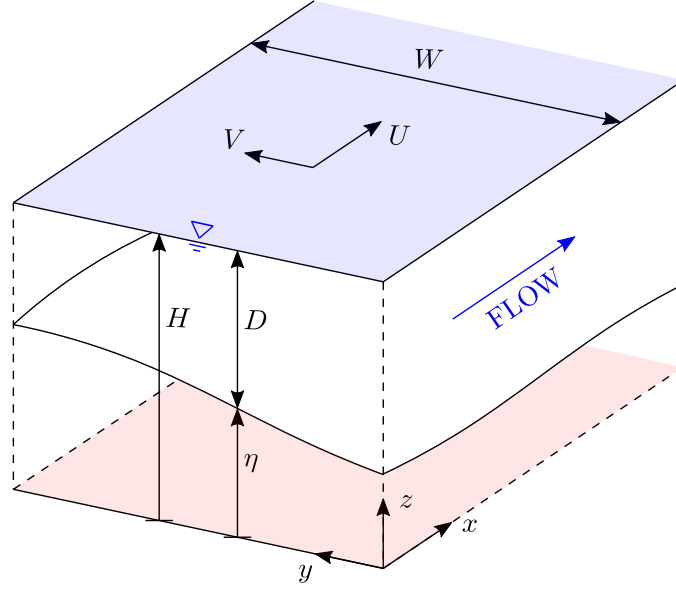


Figure 2: View of the channel of width  $W$ , showing the system of reference,  $\{x, y, z\}$ , and the two components of the velocity vector,  $\{U, V\}$ . The water surface elevation  $H$  is given by the sum of the bed elevation  $\eta$  and the water depth  $D$ . All the elevations are calculated with respect to the reference,  $z = 0$ , plane having a constant downstream gradient  $S_0$ .

132 where  $\Delta$  is the relative submerged weight of the sediment and  $\Phi$  is the dimensionless  
 133 sediment flux, which is considered to be a function of the Shields number only [e.g.  
 134 *Meyer-Peter and Muller, 1948; Parker, 1990*]. The angle of the sediment transport  
 135 vector,  $\gamma_s$ , is computed by taking into account the deflection exerted by the lateral  
 136 bed slope, by means of the following expression [e.g., *Engelund, 1981; Blondeaux and*  
 137 *Seminara, 1985*]:

$$\sin \gamma_s = \frac{qs_y}{|q\vec{s}|} = \sin \gamma_q - \frac{r}{\sqrt{\theta}} \frac{\partial \eta}{\partial y}, \quad (4)$$

138 where  $r$  is a dimensionless empirical coefficient [see *Baar et al., 2018*].

139 Despite neglecting three-dimensional flow structures, this model has been proven  
 140 to be able to capture the essential characteristics of river alternate bars, at least  
 141 in conditions where most of the sediment is transported as bedload [e.g., *Blondeaux*  
 142 *and Seminara, 1985*]. Specifically, linear solutions allow for calculating bar formation  
 143 conditions, while weakly-nonlinear and fully nonlinear theories enable for reproducing  
 144 bar height and to estimate other bar properties.

## 145 2.2 The key hypothesis

146 The present manuscript is founded on the key hypothesis that the deformation of  
 147 the free surface due to the incipient formation of bars is negligible. More precisely, we  
 148 assume that: (i) the pressure term  $g \partial H / \partial x$  in the equation of longitudinal momentum  
 149 (1a), and (ii) the variation of  $H$  when computing the bed elevation as  $\eta = H - D$   
 150 in Equations (1d) and (4), are both negligible. It is worth noticing, however, that  
 151 variations of the free surface elevation are still considered in the equation of transverse  
 152 momentum (1a), in which the pressure term  $g \partial H / \partial y$  can not be disregarded.

This hypothesis has been used to model the formation of steady alternate bars in rivers [e.g. *Struikma et al.*, 1985; *Crosato and Mosselman*, 2009], and constitutes the basis for the so-called second order models for the evolution of meandering channels [see *Camporeale et al.*, 2007]. The appropriateness of adopting this hypothesis for modelling the evolution of migrating bars is suggested by visual inspection of experimental data, where fluctuations are usually small, even at relatively high values of the Froude number *García and Niño* [1993]. Moreover, it is indirectly indicated by the weak dependence of alternate bars on Froude number [*Wilkinson et al.*, 2008], as characteristic of processes where the influence of free surface variations is small.

In the following Section 3, the comparison with the complete model and the validation against experimental data are used to demonstrate the suitability of this key hypothesis for predicting bar stability conditions. Moreover, in Section 4, we will discuss about the physical reasoning of why water surface deformation is negligible for typical hydrodynamic conditions on river bars.

### 2.3 Expression for the critical width-to-depth ratio

Neglecting the deformation of the free surface elevation allows for deriving an explicit formula for determining the possibility of migrating alternate bars to form, depending on channel characteristics and flow conditions. To this aim, we first need to specify a reference depth  $D_0$  and the associated reference Shields number  $\theta_0$ , which is given by the following uniform-flow relationship:

$$\theta_0 = \frac{S_0 D_0}{\Delta d}. \quad (5)$$

Bars formation primary depends on the channel aspect ratio, which for historical reasons is here defined as *half* the width-to-depth ratio, namely:

$$\beta = \frac{W}{2D_0}. \quad (6)$$

Specifically, when the aspect ratio exceeds a critical threshold value ( $\beta_C$ ) the initial, plane-bed configuration is unstable, and alternate bars are expected to spontaneously form [*Colombini et al.*, 1987].

A very simple formula for this critical aspect ratio can be obtained by: (i) linearizing the governing equations, (ii) considering the first mode of the Fourier expansion of the solution, (iii) analysing the time development of an initially-small bed perturbation, (iv) determining the set of parameters for which this initial perturbation tends to grow, eventually leading to finite-amplitude alternate bars. Considering that these mathematical procedure is rather standard and straightforward, we prefer avoid cluttering this section with a large number of equations. Therefore, we reported all the all the mathematical details in Appendix A , here providing only the final result of the linear stability analysis, which gives the following expression:

$$\beta_C = \frac{c_0}{2} \left[ \frac{\xi(\theta_0)}{r} (1 + 2c_D) - \frac{1}{c_0^2 \lambda^2} \right]^{-1/2}, \quad (7)$$

where the empirical coefficient  $r$  can be assumed equal to 0.3, while the dimensionless wavenumber, defined as  $\lambda = \pi W/L$  (with  $L$  indicating the bar wavelength), can be considered equal to 0.45 [*Colombini et al.*, 1987]. The symbol  $\xi$  indicates a function on the reference value of the Shields number (see Equation A.14b), which depends on the choice of the sediment transport formula. Specifically, considering the sediment transport formula of *Parker* [1978] it reads:

$$\xi(\theta_0) = \frac{\sqrt{\theta_0}}{\pi^2} \left( 9 \frac{\theta_{cr}}{\theta_0 - \theta_{cr}} + 2 \right), \quad \theta_{cr} = 0.03. \quad (8a, b)$$

193 Similarly, the reference dimensionless Chézy coefficient  $c_0$  and the associated  $c_D$  co-  
 194 efficient (equation A.6a) depends on the choice of the friction formula. Adopting the  
 195 widely-used logarithmic expression [Engelund and Hansen, 1967] gives:

$$c_0 = 6 + 2.5 \log \left( \frac{1}{2.5} \frac{D_0}{d} \right), \quad c_D = \frac{2.5}{c_0}, \quad (9)$$

196 where the ratio  $D_0/d$  represents the relative submergence. Alternatively, the friction  
 197 coefficients can be calculated from the Manning formula as follows:

$$c_0 = \frac{D_0^{1/6}}{n\sqrt{g}}, \quad c_D = 1/6, \quad (10)$$

198 where the Manning coefficient  $n$  needs to be estimated on the basis of the bed rough-  
 199 ness.

## 200 3 Results

### 201 3.1 Why do bars form? A physical explanation

202 The hypothesis of negligible variations of the water surface elevation allows for a  
 203 great simplification of the problem, as needed to physically understand the mechanisms  
 204 that drive the formation and suppression of free alternate bars.

#### 205 *The bar-forming mechanism*

206 We consider the depth-averaged Equation of the streamwise momentum (1a),  
 207 where we neglect the transverse flux of longitudinal momentum (second term), as  
 208 appropriate when studying the initial stages of bar development (see Appendix A ):

$$U \frac{\partial U}{\partial x} = gS_0 - g \frac{\partial H}{\partial x} - \frac{\tau_x}{\rho D}. \quad (11)$$

209 By discarding the term related to the water surface deformation (i.e. according to our  
 210 fundamental hypothesis), the above Equation (11), once multiplied by  $\rho D$ , reads:

$$\underbrace{\rho U D \frac{\partial U}{\partial x}}_{\text{Inertia}} = \underbrace{\rho g D S_0}_{\text{Weight}} - \underbrace{\tau_x}_{\text{Friction}}, \quad (12)$$

211 which simply states that any imbalance between the longitudinal component of the  
 212 water weight and the bottom friction necessarily produces a flow acceleration or de-  
 213 celeration.

214 In plane-bed conditions the flow is uniform, weight and friction keep in balance  
 215 (i.e.  $\tau_x = \rho g D S_0$ ) and no acceleration/deceleration occur. In this case, the sediment  
 216 transport is also uniform, so that neither erosion nor deposition appear. Conversely,  
 217 if a three-dimensional perturbation of the bed is introduced, the flow is no longer  
 218 uniform. Let us consider for example a deposition patch on one side of the channel  
 219 (i.e. a three-dimensional bed disturbance), having a length of several times the channel  
 220 width and an initially-small height (Figure 3). Since the free surface deformation is  
 221 negligible, the depth over the deposition patch does clearly reduce, and the weight of  
 222 the water column decreases. Considering that the friction term does not substantially  
 223 change until the flow velocity varies (it is actually possible to assume  $\tau_x$  to be constant,  
 224 as discussed later), the decrease of weight does necessarily produce a flow deceleration  
 225 ( $\partial U / \partial x < 0$ ). This implies a spatial decrease in the sediment flux and an associated  
 226 deposition, which increases the height of the initial bed disturbance. This represents  
 227 a self-sustained instability mechanism, which ultimately leads to the formation of the  
 228 large-scale, finite-amplitude bedforms called free bars.

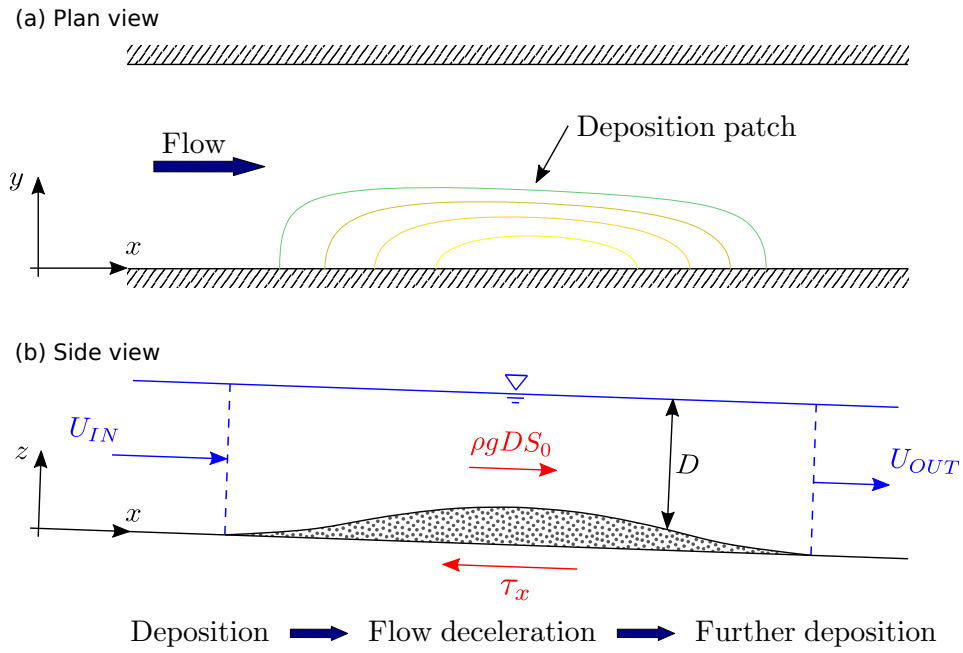


Figure 3: Illustration of the physical mechanism that sustains the bar growth. The generic, initially-small, three-dimensional deposition patch located near the right bank (see contour lines in the plan view) produces a decrease of the local water depth ( $D$ ) and an associated reduction of tracting force due to the weight of the water column ( $\rho g D S_0$ ). The imbalance between the reduced water weight and the bed friction  $\tau_x$  necessarily produces a flow deceleration ( $U_{OUT} < U_{IN}$ ), which induces further deposition, thus producing a self-sustained bar growth.

It is worth highlighting that the above-described mechanism is only valid for a three-dimensional bed perturbation, where the flow has enough space to move laterally around the obstacle without significant deformations of the free surface. Conversely, if the bed perturbation was purely two-dimensional, the flow would be obliged to entirely transit over the bedform, and the momentum balance would be affected by the pressure terms associated with the variations of the free surface. In these conditions, the shallow-water-Exner model invariably gives a suppression of the perturbation, which indicates that the basic uniform flow is always stable.

### *The bar-suppressing mechanism*

The main contrasting mechanism is due to the gravitational effect on the direction of the bedload transport: the sediment tends to be deviated by an angle  $\gamma_s$  that depends on the lateral slope according to Equation (4). As illustrated in Figure 4 this deviation produces a transverse sediment flux towards the lower part of the cross-section (bar pools). This mechanism tends to suppress three-dimensional bedforms, eventually leading to flat-bed conditions if no other, constructive forces exist.

Specifically, the transverse flux of sediment ( $qs_y$ ) predicted by Equation (4) is proportional to the lateral slope  $\partial\eta/\partial y$ . This represents the characteristic relation of diffusive processes, where the mass flux depends on the gradient, and is directed in the opposite direction [e.g., Crank, 1975]. As any diffusive process, the bed adaptation follows a timescale that is proportional to the square of the domain size (i.e.  $T \propto W^2$ ). For example, considering a purely transverse bed deformation (no variations along the longitudinal direction - no constructive forces) the time needed to attain flat-bed conditions is proportional to the square of the channel width. Ultimately, this is the reason for which an exponent  $-1/2$  appears in the expression for the critical aspect ratio (7) (i.e. the stability condition depends on the square of  $\beta$ , see also Equation (A.14)).

In physical terms, this quadratic dependence can be easily understood by considering that channel width as a twofold effect. On the one side, transverse bed gradient and the associated transverse flux of sediment are inversely proportional to the channel width. On the other hand, the volume of sediments that needs to be laterally transferred is proportional to the width itself. Therefore, bed flattening in wider channel needs to a larger mass transfer with a lower flux, therefore requiring a much longer time.

## **3.2 When do alternate bars form? Results from the simplified criterion**

The explicit expression for the critical aspect ratio (7) derived above provides a simple criterion for bar formations. Specifically, migrating alternate bars are predicted to form when the aspect ratio  $\beta$  exceeds the critical threshold  $\beta_C$ , while in the opposite case plane-bed conditions are expected, despite the possible development of low-relief oblique dunes [e.g., Redolfi *et al.*, 2020] or other kind of small-scale bedforms.

As illustrated in Figure 5, the critical aspect ratio tends to initially increase with the Shields number while it tends to slightly decrease when  $\theta_0$  exceeds 0.21, value at which the function  $\xi(\theta_0)$  is minimum. Moreover,  $\beta_C$  significantly increases for higher values of the relative submergence, which according to Equation (9) are associated with higher values of the Chézy coefficient  $c_0$ . In general, predictions by our simplified expression are very similar to those resulting from the complete model of Colombini *et al.* [1987]. Specifically, the critical aspect ratio shows a maximum relative error of 2.8% (for relatively high  $\theta_0$  and the low  $D_0/d$ ), which seems acceptable for most applications.

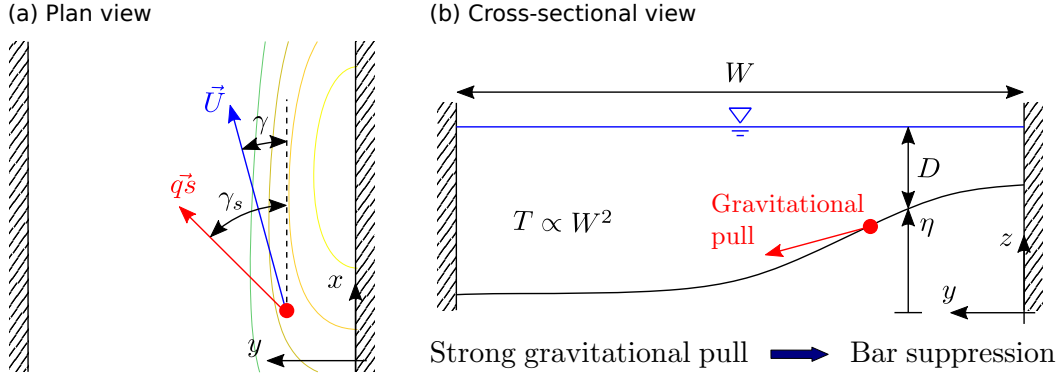


Figure 4: Effect of the gravitational pull on a laterally-sloping bed, which produces a downward deviation of the sediment flux  $\vec{q}s$  with respect to the flow velocity vector  $\vec{U}$  as illustrated in the plan view (a). As a result, the sediment flux tends to laterally move towards the most depressed areas, as illustrated in the cross-sectional view (b), which tends to flatten the bed. The timescale of the bed adaptation ( $T$ ) is proportional to the square of the channel width ( $W$ ) as typical of diffusive processes, which makes the bar-suppressing mechanism much more effective in relatively narrow channels.

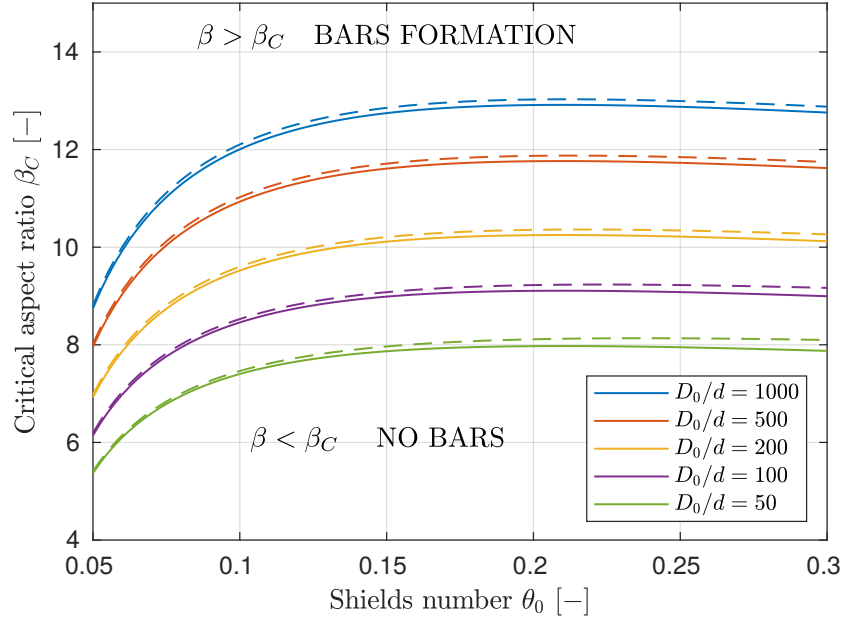


Figure 5: Critical aspect ratio resulting from the complete model of *Colombini et al.* [1987] (dashed lines) and by Equation (7) (solid lines), depending on Shields parameter ( $\theta_0$ ) and relative submergence ( $D_0/d$ ). Migrating alternate bars are expected to form when the channel aspect ratio  $\beta = W/(2D_0)$  exceeds the critical threshold  $\beta_C$ . The maximum relative error of the simplified model is 2.8%, which reduces to 1.6% when limiting the space of parameters to cases for which the Froude number is lower than 1.

277 A further simplification can be obtained by neglecting the term  $1/(c_0^2\lambda^2)$  in Equa-  
 278 tion (7), which gives a wavelength-independent stability condition. From a physical  
 279 point of view, this means discarding the effect of velocity variations on the bed shear  
 280 stress  $\tau_x$ . If compared with the complete model of *Colombini et al.* [1987] this fur-  
 281 ther reduced model leads to a maximum relative error of 4.5% within the range of  
 282 parameters of Figure 5, which reduces to 3.2% when focussing on  $Fr < 1$  cases only.  
 283 Ultimately, a maximal simplification arises when considering also  $c_D = 0$ , which im-  
 284 plies assuming spatially invariant bed shear stress (i.e.  $\tau_x = const$ ). Though this may  
 285 appear as an extreme hypothesis, it actually leads to an maximum relative error of  
 286 about 16% with respect to the complete model.

### 287 *Comparison against experimental data*

288 Comparison between our formula and experimental data is performed by con-  
 289 sidering the dataset reported by *Colombini et al.* [1987], encompassing experimental  
 290 data from *Kinoshita* [1961]; *Ashida and Shiomi* [1966]; *Chang et al.* [1971]; *Sukegawa*  
 291 [1971]; *Muramoto and Fujita* [1978]; *Ikeda* [1982]; *Jäggi* [1983] here expanded by in-  
 292 cluding the more recent laboratory experiments by [*García and Niño*, 1993; *Lan-*  
 293 *zoni*, 2000; *Ahmari and Da Silva*, 2011; *Crosato et al.*, 2011; *Garcia Lugo et al.*, 2015;  
 294 *Redolfi et al.*, 2020], for a total of 416 experiments. Alternate bars were observed in  
 295 288 cases, where in the remaining 128 either plane bed or other bedforms (dunes,  
 296 antidunes or diagonal bars) are observed.

297 As illustrated in Figure 6 our simple equation is able to correctly classify most  
 298 of the experimental outcomes, as most of the experiments with alternate bars fall in  
 299 the region  $\beta > \beta_C$  while the remaining cases are often characterized by  $\beta < \beta_C$ . More  
 300 specifically, 364 experiments (87.5%) are correctly classified, 35 (8.4%) can be desig-  
 301 nated as “false negatives” (bars are observed to form, despite  $\beta < \beta_C$ ) and 17 (4.1%)  
 302 “false positive” (bars do not develop, despite  $\beta > \beta_C$ ). It is worth highlighting that  
 303 this result is obtained without any specific calibration of the empirical coefficient  $r$   
 304 or distinct choice of the sediment transport formula. In this sense, additional infor-  
 305 mations about the sediment transport (e.g., measured transport rate) would enable  
 306 for specifically calibrating the model parameters for each set of experiments, which is  
 307 expected to improve the overall accuracy of the predictions.

308 The capability of our formula to reproduce experimental results is then compared  
 309 with analogue results from the application of the complete model and of the empiri-  
 310 cal criteria by *Muramoto and Fujita* [1978], *Jaeggi* [1984], *Yalin and Da Silva* [2001]  
 311 and *Ahmari and Da Silva* [2011], whose expressions are reported in Appendix B . To  
 312 this aim we first consider classic indicators of classification performance, namely the  
 313 accuracy (ACC) and the balanced accuracy (BA) [see *Tharwat*, 2018]. We considered  
 314 all the experimental data, except those having a severely limited bed mobility, due to  
 315 low Shields number ( $\theta_0 < 0.03$ ) or bed armouring. Results reported in Table 1 sug-  
 316 gest that our formula gives substantially the same performance as the complete model  
 317 of *Colombini et al.* [1987], which is overall better with respect to the other empirical  
 318 criteria.

319 The above accuracy indicators are merely based on a binary (bars-no bars) classi-  
 320 fication but do not take into account the “degree of stability” predicted by the different  
 321 cases. For example, experiments that are very close to the threshold are expected to be  
 322 easily misclassified, so that an error in this case is less important than a classification  
 323 error for highly stable or unstable conditions. To overcome this limitation, we propose  
 324 an indicator that accounts for the (logarithmic) distance of the incorrectly-classified  
 325 measurements from the critical threshold:

$$dev = \frac{\sum_{\{FP, FN\}} |\log(\beta/\beta_C)|}{\sum |\log(\beta/\beta_C)|}, \quad (13)$$

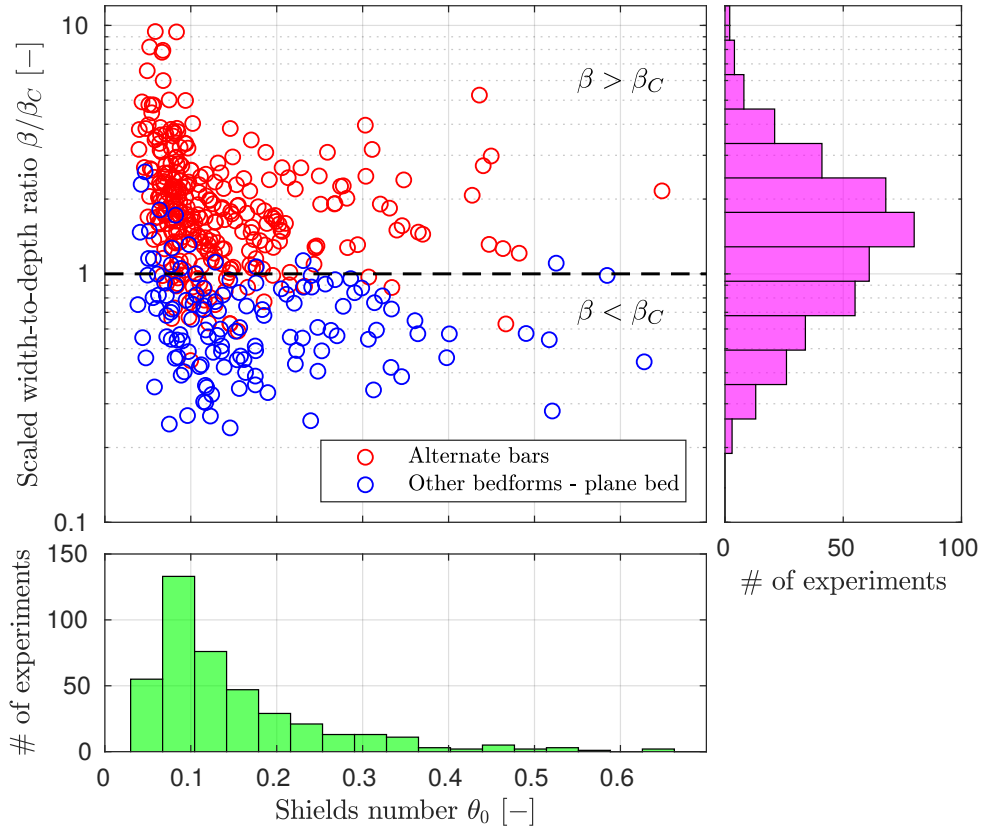


Figure 6: Comparison between our bar formation criterion and the dataset of laboratory experimental observations. Red circles indicate conditions at which alternate bars were observed, while blue circles refers to other bed configurations, including plane-bed, diagonal bars, dunes and antidunes. Free alternate bars are expected to form when points fall above the dashed line that indicates the critical aspect ratio  $\beta_C$ . The histograms represent the frequency distribution of the experiments depending on Shields number (lower plot) and scaled width-to-depth ratio  $\beta/\beta_C$  (right plot).

Table 1: Classification performances of different bar predictors. ACC indicates the accuracy, BA the balanced accuracy.

	ACC	BA	dev
<i>Muramoto and Fujita</i> [1978]	83.2%	86.1%	8.1%
<i>Jaeggi</i> [1984]	80.3%	82.3%	15.8%
<i>Yalin and Da Silva</i> [2001]	77.4%	64.6%	11.8%
<i>Ahmari and Da Silva</i> [2011]	75.2%	61.3%	11.7%
<i>Colombini et al.</i> [1987]	87.0%	87.2%	5.2%
Present formula (7)	87.5%	87.3%	5.0%

326 where FP and FN indicate the set of false positive and false negative results, so that  
327 *dev* ranges from zero to one, with lower values indicating a good prediction. Values  
328 reported in Table 1 show that our formula provides similar results as the complete  
329 model of *Colombini et al.* [1987], with significantly less deviation than the other exist-  
330 ing criteria.

## 331 4 Discussion

332 In this work we provide a novel explanation of the physical mechanism that  
333 leads to the spontaneous formation of free alternate bars in rivers. Surprisingly, this  
334 mechanisms turns out to be extremely simple, to the point that it can be described  
335 as an unbalance between water weight and bottom friction, which causes deceleration  
336 near the top of bars and consequent further deposition. Specifically, the analysis of  
337 the two-dimensional solution of the shallow water model is to some extent simpler  
338 than its one-dimensional counterpart, as in the latter pressure terms due to the water  
339 surface deformation are rarely negligible. The bar formation is clearly counteracted by  
340 the effect of the lateral slope on the sediment transport, which tends to suppress bars  
341 [*Fredsoe, 1978; Seminara, 2010*]. In this perspective, our analysis highlights the strong  
342 (i.e. quadratic) dependence of this effect on the channel width, which represents the  
343 hallmark of diffusive processes.

344 Neglecting variations of the free surface elevation allows for obtaining an ex-  
345 plicit expression for calculating the critical width-to-depth ratio with an error of a few  
346 percent with respect to the complete model of *Colombini et al.* [1987]. Comparison  
347 with an unprecedented number of laboratory experiments, encompassing more than  
348 400 experimental runs from the existing literature, reveal that our explicit formula  
349 enables for predicting the bar formation in the vast majority of cases. Specifically,  
350 the resulting accuracy is comparable to that of the complete model and better with  
351 respect to existing empirical criteria. It is not our intention here to discuss what is the  
352 best criteria, as the answer is likely to depend on the specific objective of the analysis,  
353 on the availability of data and on the field of application. However, we find relevant to  
354 here highlight the main strengths of physically-based expressions, which are directly  
355 derived from the equations of Newtonian mechanics through well-defined and testable  
356 assumptions. Following this reductionist approach [see *Seminara and Bolla Pittaluga,*  
357 *2012*], the effect of all the essential parameters, including those that are normally fixed  
358 (e.g., the gravitational acceleration) is embodied, and can be directly associated with  
359 the underlying physical processes. In particular, our derivation allows for clarifying  
360 the following effects:

- 361 • the decrease of the critical aspect ratio for lower values of the relative submer-  
362 gence  $D/d$  (i.e. for low values of the Chézy parameter  $c_0$ ) can be mechanically

363 explained by considering that to maintain comparable values of Shields number  
 364 and water depth on a rough bed, weight and bottom friction need to be higher  
 365 (i.e. the slope must be higher). In such conditions, any unbalance between  
 366 the two terms on the right hand side of Equation (12) is expected to produce  
 367 a stronger accelerations/decelerations, which reinforces the bar-forming mecha-  
 368 nism;

- 369 • the Shields number shows two distinct and opposite effects. On the one side,  
 370 increasing  $\theta_0$  makes the bar-forming mechanism less effective, as it reduces the  
 371 sensitivity of the sediment transport to variations of velocity (i.e. the coef-  
 372 ficient  $\Phi_T$ , see Appendix A ). On the other side, increasing  $\theta_0$  weakens the  
 373 bar-suppressing mechanism, as it reduces the deflection of the sediment trans-  
 374 port predicted by Equation 4. While the former effect dominates at moderate  
 375 values of the Shields number, the latter prevails when  $\theta_0 > 0.21$ , which explains  
 376 the non-monotonic trend of  $\beta_C$  appearing in Figure 5;
- 377 • higher values of the empirical parameter  $r$  enhance the bar-suppressing mecha-  
 378 nism, as they are associated with a stronger deflection of the sediment transport  
 379 (see again Equation (4)). Therefore, the critical aspect ratio clearly increases  
 380 with  $r$ .

381 Knowing the effect of all the individual parameters allows for adapting the formula to  
 382 the specific sediment transport and flow friction conditions, by assimilating information  
 383 from measurements or antecedent studies. For example, if field calibrated values of the  
 384 Manning coefficient are available it is possible to bypass Equation (9a), and to directly  
 385 compute  $c_0$  from the Manning coefficient. This may be particularly important for the  
 386 design and the interpretation of numerical simulations as in this case our formula can  
 387 be adapted to consider the same friction and sediment transport formulas, and exactly  
 388 the same value of the parameter  $r$ .

#### 389 4.1 The key hypothesis: physical reasoning and limitations

390 The appropriateness of neglecting free surface deformations is evident from the  
 391 comparison between results of the simplified and the complete model illustrated above.  
 392 However, here we would like to analyse the reason for which this hypothesis can be  
 393 accepted, depending on the characteristics scales of the problem. A reader who is not  
 394 interested to deepen this topic can directly jump to Section 4.2.

395 The validity of this hypothesis for modelling steady bars has been justified by  
 396 *Struiksmma et al.* [1985] by considering that when the Froude number is small, variations  
 397 of the free surface elevation are small with respect to variations of the bed elevation.  
 398 In these conditions it is possible to introduce the so-called rigid-lid assumption, which  
 399 allows for computing variations of water depth on the basis of variations of the bed  
 400 topography. However, this does not explain why variations of the free surface elevation  
 401 can be neglected from the longitudinal momentum balance (1a), as the term  $g \partial H / \partial x$   
 402 generally remains finite when  $Fr \rightarrow 0$ , representing the pressure gradient that appears  
 403 under the rigid-lid assumption. For this reason, we found important to further discuss  
 404 the possibility to neglect this term when modelling free migrating bars (present paper)  
 405 and steady bars [*Crosato and Mosselman, 2009; Camporeale et al., 2007*].

406 Here we show that this simplification is generally valid for the case of three-  
 407 dimensional bed deformations having a longitudinal scale of several channel widths,  
 408 as typically the case of all river alternate bars. Though this can be demonstrated by  
 409 a mathematically rigorous perturbation approach, an analogous result can be found  
 410 by simply evaluating the order of magnitude of the main terms of the fundamental  
 411 conservation equations. Specifically, if we denote with  $\tilde{D}$  and  $(\tilde{U}, \tilde{V})$  the order of

412 magnitude of the depth and velocity components, the continuity Equation (1a) gives:

$$\frac{\tilde{V}\tilde{D}}{\Delta\tilde{y}} \sim \frac{\tilde{U}\tilde{D}}{\Delta\tilde{x}}, \quad (14)$$

413 where  $\Delta\tilde{x}$  and  $\Delta\tilde{y}$  are the longitudinal and the transverse scales of variation. Indicating  
414 with  $\Lambda$  the ratio  $\Delta x/\Delta y$ , Equation (14) can be expressed as:

$$\tilde{V} \sim \frac{\tilde{U}}{\Lambda}, \quad (15)$$

415 which reveals that the magnitude of the transverse velocity decreases with the longi-  
416 tudinal scale.

417 The Equation of transverse momentum (1b) suggests that transverse acceleration  
418 and lateral inclination of the free surface have the same order magnitude, namely:

$$g \frac{\Delta\tilde{H}}{\Delta\tilde{y}} \sim \tilde{U} \frac{\tilde{V}}{\Delta\tilde{x}}, \quad (16)$$

419 where  $\Delta\tilde{H}$  indicates the order of magnitude of the free surface variations. Combining  
420 equations (16) and (15) gives:

$$g \frac{\Delta\tilde{H}}{\Delta\tilde{x}} \sim \tilde{U} \frac{\tilde{V}}{\Delta\tilde{x}} \frac{1}{\Lambda} \sim \tilde{U} \frac{\tilde{U}}{\Delta\tilde{x}} \frac{1}{\Lambda^2}, \quad (17)$$

421 which implies that the gravitational term in the equation of longitudinal momentum  
422 (1a) is negligible when  $\Lambda$  is sufficiently large. The above condition (17) can be equiv-  
423 alently expressed in the Froude number as follows:

$$\frac{\Delta\tilde{H}}{\tilde{F}r^2\tilde{D}} \sim \frac{1}{\Lambda^2}, \quad \tilde{F}r^2 := \frac{\tilde{U}^2}{g\tilde{D}}, \quad (18a, b)$$

424 To test this conclusion we consider a periodic, double-sinusoidal bed deformation  
425 of amplitude  $A$  and wavelength  $L$  (Figure 7a). In this case the longitudinal and  
426 transverse scales of variations ( $\Delta\tilde{x}$  and  $\Delta\tilde{y}$ ) can be quantified as the distance between  
427 wave crest and trough ( $L/2$  and  $W$ ), so that their ratio  $\Lambda$  is given by  $L/(2W) = \pi/(2\lambda)$ .  
428 We then computed the two-dimensional flow field by analytically solving Equations  
429 (1a,b,c) under the hypothesis of small perturbations (linear analysis), by varying the  
430 wavelength of the bed oscillation ( $L$ ) and the Froude number  $Fr$ , keeping all the other  
431 flow parameters invariant. Results illustrated in Figure 7 confirm that when increasing  
432 the value  $L/W$  (i.e. the value of  $\Lambda$ ) transverse velocity and variations of the water  
433 surface elevation decrease, as predicted by Equations (15) and (17). Moreover, for  
434 characteristic wavelengths of migrating bars ( $L/W$  from 5 to 12, with typical value  
435 around 7, corresponding to  $\lambda = 0.45$ ) and steady bars ( $L/W > 12$ ) the complete  
436 solution is nearly independent of the Froude number, and is correctly reproduced  
437 by the simplified model, which corroborates the hypothesis of negligible free surface  
438 deformation.

439 This explains why alternate bars are essentially independent of the Froude num-  
440 ber, to the point that they are weakly sensitive to the transition from sub- to super-  
441 critical flow regimes [Wilkinson *et al.*, 2008]. In this perspective, it is interesting  
442 to notice that this property has been recently observed by Ragno *et al.* [2021] for  
443 bifurcation-confluence loops, where the river splits in two anabranches than then re-  
444 join downstream. This suggests that the weak dependence on the Froude number may  
445 represent a rather general, remarkable property of three-dimensional morphodynamic  
446 systems, such as multi-thread braided rivers, where the water flow is free to laterally  
447 move across bars and among different anabranches.

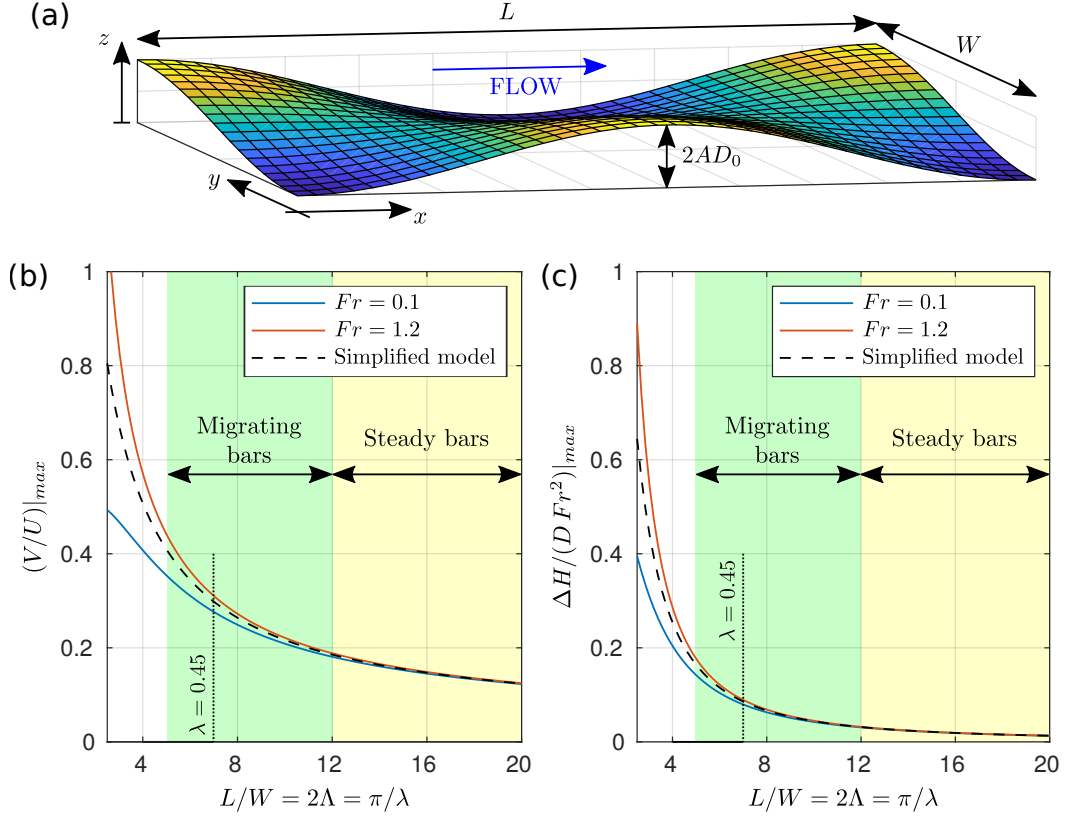


Figure 7: Effect of the bar wavelength on transverse velocity ( $V$ ) and water surface deformation ( $\Delta H$ ), obtained by imposing a double-sinusoidal bed deformation of dimensionless amplitude  $A$  and wavelength  $L$  (a), and solving the linearized shallow water equations. Specifically, panels (b) and (c) report maximum values of  $V/U$  and  $\Delta H / (Fr^2 D)$  for increasing values of  $L/W$ , considering an unitary dimensionless amplitude and two extreme values of the reference Froude number  $Fr$ . The solid lines refer to the complete linear solution, while the dashed line indicates the (Froude-independent) solution from the simplified model. For the typical wavelength of migrating and steady bars (shaded areas) the three lines tend to converge, which indicates the appropriateness of the fundamental hypothesis. The dotted line indicates the wavelength  $\lambda = 0.45$  we adopted when applying Equation (7). Example with  $\beta = 12$  and  $D/d = 100$ .

448 Similarly, the present analysis justifies why shorter three-dimensional bedforms  
 449 like oblique dunes or diagonal bars [see *Colombini and Stocchino, 2012*] are instead  
 450 significantly influenced by the Froude number. This is also the case of two-dimensional  
 451 bed deformations, for which the independence of the Froude number is achieved only  
 452 when the length scale of the bed slope variations is longer than the length of the  
 453 backwater profiles (i.e. the so-called backwater length), so that the flow inertia is  
 454 negligible and the morphological evolution is essentially diffusive [e.g., *Paola, 2000*;  
 455 *Redolfi and Tubino, 2014*; *Shaw and McElroy, 2016*].

456 Ultimately, this analysis reveals that the model simplification adopted in this  
 457 manuscript is possible thanks to the peculiar characteristic of bars being long, three  
 458 dimensional bedforms, which allows the flow to deflect around bars without produc-  
 459 ing significant deformations of the water surface, even at moderate Froude numbers.  
 460 For this reason, this hypothesis is usually not satisfied for two-dimensional bed de-  
 461 formations, for which the flow is obliged to surmount the bedforms, thus producing  
 462 mechanically significant variations of the free surface.

## 463 4.2 Limitations and future perspectives

464 This work demonstrates that neglecting variations of the free surface elevation  
 465 allows for a satisfactory prediction of the alternate bar formation. However, it is worth  
 466 highlighting that, differently from the complete linear theories [e.g. *Colombini et al.,*  
 467 *1987*], our model does not enable to determine the bar wavelength, because it predicts  
 468 a monotonically-increasing instability for decreasing bar wavelength. This is clearly  
 469 related to the fact that, as demonstrated above, the key assumption is not valid for  
 470 relatively short wavelengths. However, this limitation does not prevent for an accurate  
 471 prediction of the critical aspect ratio, for two reasons: (i) the wavenumber resulting  
 472 from complete theories is relatively constant, so that its average value  $\lambda = 0.45$  can be  
 473 considered representative; (ii) the critical aspect ratio is weakly sensitive to variations  
 474 of the wavenumber, to the point that even setting  $\lambda \rightarrow \infty$  in Equation (7) gives an  
 475 error of a few percent only.

476 Our expression for the marginal stability condition is meant for predicting the  
 477 formation of alternate (i.e first mode) bars only, and does not provide indications about  
 478 the transition to higher bar modes (i.e. central or multiple-row bars) that is expected  
 479 in wider channels [*Fredsoe, 1978*; *Crosato and Mosselman, 2009*]. Our approach can  
 480 be easily extended to predict the growth rate of higher modes, and would allow to  
 481 determine the most unstable bar mode depending on conditions [see *Tubino et al.,*  
 482 *1999*]. However, this clearly goes beyond the purpose of the paper.

483 When applying our criterion to river, the following question arises: “how to se-  
 484 lect an appropriate value of dominant, formative discharge that can be adopted to  
 485 represent the bar response?”. Previous works usually rely on either the bankfull dis-  
 486 charge [e.g., *Crosato and Mosselman, 2009*; *Ahmari and Da Silva, 2011*; *Crosato and*  
 487 *Mosselman, 2020*] or on the discharge with 2-year return period [e.g., *Adami et al.,*  
 488 *2016*], as commonly suggested for reproducing river morphodynamic processes. How-  
 489 ever, a specific methodology to derive formative conditions for migrating bars has been  
 490 recently proposed by *Carlin et al. [2021]*, who suggested that the possibility of bars to  
 491 form depends on the average growth rate, calculated by considering all the possible  
 492 discharge states, namely:

$$493 \quad \bar{\Omega} = \int_0^{\infty} \Omega f_Q dQ, \quad (19)$$

494 where  $f_Q$  indicates the probability density function of the flow events. In this perspec-  
 495 tive, our work analysis provides all the necessary information for directly computing  
 the bar growth rate  $\Omega$  as a function of discharge by means of Equation (A.13).

496 Finally, the present analysis is limited to conditions where most of the sediment  
 497 is transported as bedload, as reproducing the effect of suspended load on bar stability  
 498 requires a more sophisticated model, based on either a non-equilibrium stress-transport  
 499 relation [*Federici and Seminara, 2006; Bertagni and Camporeale, 2018*] or on a fully  
 500 three-dimensional approach [*Tubino et al., 1999*]. However, our model allows for qual-  
 501 itatively explaining the increase of bar instability in observed in suspension-dominated  
 502 channels: since the suspended load is substantially not affected by the gravitational  
 503 pull predicted by Equation (4), the bar suppressing mechanisms is expected to be  
 504 weaker, which promotes bar formation.

## 505 5 Conclusions

506 Neglecting the deformation of the water surface in the classic two-dimensional  
 507 shallow water and Exner model allowed for a considerable simplification of the math-  
 508 ematical description of the process of bar formation, which facilitated the physical  
 509 understanding of the phenomenon. This led to the following conclusions:

- 510 • The physical mechanism that leads to a self-sustained development of free mi-  
 511 grating bars is surprisingly simple, as it results from an imbalance between wa-  
 512 ter weight and bottom friction. Specifically, if a three-dimensional, depositional  
 513 patch is introduced, water depth and associated weight reduce, which produces  
 514 a flow deceleration and further deposition. This bar-forming instability pro-  
 515 cess tends to be counteracted by the effect of the gravitational pull on the bed  
 516 particle transported as bed load. The importance of this bar-suppressing effect  
 517 increases quadratically when reducing the channel width, which explains why  
 518 bar formation is strongly discourages when the channel width-to-depth ratio is  
 519 low.
- 520 • An explicit, physically-based formula for predicting conditions for the formation  
 521 of migrating alternate bars can be derived. Testing based on a very large number  
 522 of laboratory experiment, suggests that the formula we propose is on average  
 523 more accurate than existing empirical predictors. Moreover, the physically-  
 524 based derivation of the formula allows for assessing the effect of all the essential  
 525 parameters that concur in determining the bar stability, and it therefore suitable  
 526 to be adapted and extended to a wide range of conditions.
- 527 • The hypothesis of negligible deformation of the water surface is intimately re-  
 528 lated to two essential characteristics of bars: (i) the three-dimensional structure;  
 529 (ii) the long longitudinal extension, which allow for a gentle deviation of the flow,  
 530 without significant variations of the water surface elevation. For this reason it  
 531 does not apply to two-dimensional or comparatively short three-dimensional  
 532 bedforms, such as two-dimensional dunes or oblique dunes. Ultimately, this  
 533 hypothesis implies a that the Froude number plays a negligible role in the for-  
 534 mation of bars. This suggests that a substantial independence of the Froude  
 535 parameter may be a general, remarkable property of all morphodynamics sys-  
 536 tems characterized by a three-dimensional bed topography, such as multi-thread  
 537 braided rivers.

## 538 Appendix A Derivation of an explicit expression for the critical as- 539 pect ratio

540 The linear stability analysis of the system of partial differential equations (1) is  
 541 obtained by considering small perturbations with respect to a reference, undisturbed  
 542 flow, here denoted with the subscript  $_0$ . Specifically, we consider an expression of the

543 dependent variables in the form:

$$U = U_0 [1 + U_1^*], \quad (\text{A.1a})$$

$$V = U_0 [0 + V_1^*], \quad (\text{A.1b})$$

$$D = D_0 [1 + D_1^*], \quad (\text{A.1c})$$

$$H = D_0 [0 + H_1^*], \quad (\text{A.1d})$$

544 where  $U_1^*, V_1^*, D_1^*, H_1^*$  represent the dimensionless perturbations.

545 Moreover, it is convenient to express also the independent variables in dimensionless form. Specifically, planimetric coordinates are scaled with half the channel width *Colombini et al.* [1987], namely:

$$x^* = \frac{x}{W/2}, \quad y^* = \frac{y}{W/2}, \quad (\text{A.2a, b})$$

548 while time is made dimensionless by means of the Exner timescale (i.e. that naturally arising from the sediment continuity equation), namely:

$$t^* = t \frac{qs_0}{(1-p)D_0W/2}. \quad (\text{A.3})$$

550 Substituting the above expressions in the system of four differential equations (1), considering the closure relations (2-4), and neglecting the nonlinear terms, gives the following linear system:

$$\frac{\partial U_1^*}{\partial x^*} + \frac{1}{Fr^2} \frac{\partial H_1^*}{\partial x^*} + \frac{\beta}{c_0^2} [2U_1^* - D_1^* (1 + 2c_D)] = 0, \quad (\text{A.4a})$$

$$\frac{\partial V_1^*}{\partial x^*} + \frac{1}{Fr^2} \frac{\partial H_1^*}{\partial y^*} + \frac{\beta}{c_0^2} V_1^* = 0, \quad (\text{A.4b})$$

$$\frac{\partial D_1^*}{\partial x^*} + \frac{\partial U_1^*}{\partial x^*} + \frac{\partial V_1^*}{\partial y^*} = 0, \quad (\text{A.4c})$$

$$\frac{\partial (H_1^* - D_1^*)}{\partial t^*} + \frac{\partial V_1^*}{\partial y^*} - \frac{r}{\beta\sqrt{\theta_0}} \frac{\partial^2 (H_1^* - D_1^*)}{\partial y^{*2}} + 2\Phi_T \frac{\partial U_1^*}{\partial x^*} - 2\Phi_T c_D \frac{\partial D_1^*}{\partial x^*} = 0, \quad (\text{A.4d})$$

553 where the reference Froude number and aspect ratio are given by:

$$Fr = \frac{U_0}{\sqrt{gD_0}}, \quad \beta = \frac{W/2}{D_0}. \quad (\text{A.5a, b})$$

554 The dimensionless coefficients  $\Phi_T$  and  $c_D$ , which measure the nonlinearity of the response of bedload and flow resistance to variations of Shields stress and water depth, are defined as:

$$\Phi_T := \frac{\theta_0}{\Phi_0} \frac{\partial \Phi}{\partial \theta} \Big|_{\theta=\theta_0}, \quad c_D := \frac{D_0}{c_0} \frac{\partial c}{\partial D} \Big|_{D=D_0}, \quad (\text{A.6a, b})$$

557 and their explicit expression depends on the choice of the sediment transport and friction formulae.

559 The spatial variations of the free surface elevations, can be neglected from the water and sediment continuity equations, and from the longitudinal momentum equations (red-crossed terms). Conversely, they are still important to satisfy the equation of transverse momentum, as the water surface deformation is needed to guide the lateral flow movement. However, this simplification allows for decoupling the problem, as Equations (A.4a,c,d) can be resolved independently from Equation (A.4b). Moreover, isolating the term  $\partial V_1^*/\partial y$  from the water continuity Equation (A.4c) and substituting it into the Exner equation (A.4d) allows for reducing Equations (A.4a,c,d) into the following differential system of two equations in the two unknowns  $U_1$  and  $D_1$ :

$$\frac{\partial U_1^*}{\partial x^*} + \frac{\beta}{c_0^2} [2U_1^* - D_1^* (1 + 2c_D)] = 0, \quad (\text{A.7a})$$

$$-\frac{\partial D_1^*}{\partial t^*} - \frac{\partial D_1^*}{\partial x^*} - \frac{\partial U_1^*}{\partial x^*} + \frac{r}{\beta\sqrt{\theta_0}} \frac{\partial^2 D_1^*}{\partial y^{*2}} + 2\Phi_T \frac{\partial U_1^*}{\partial x^*} - 2\Phi_T c_D \frac{\partial D_1^*}{\partial x^*} = 0. \quad (\text{A.7b})$$

568 Considering the simplified shallow water equations, we look for a wavelike so-  
 569 lution where spatial variations assume the form of a double sinusoid as illustrated in  
 570 Figure 7a. Specifically:

$$U_1^* = \hat{u} \exp [i\lambda x^* + (\Omega - i\omega)t^*] \cos(\pi y^*/2) + c.c., \quad (\text{A.8a})$$

$$D_1^* = \hat{d} \exp [i\lambda x^* + (\Omega - i\omega)t^*] \cos(\pi y^*/2) + c.c., \quad (\text{A.8b})$$

571 where  $\hat{u}$  and  $\hat{d}$  are complex coefficients,  $i = \sqrt{-1}$  denotes the imaginary unit, *c.c.*  
 572 indicates the complex conjugate. The real coefficients  $\Omega$  and  $\omega$  represent the dimen-  
 573 sionless growth rate and angular frequency, while  $\lambda$  is the dimensionless longitudinal  
 574 wavenumber, defined as  $\lambda = \pi W/L$ , where  $L$  is the bar wavelength [see *Colombini*  
 575 *et al.*, 1987].

576 Substituting Equation (A.8) into the system of linear Equations A.7 leads to a  
 577 system of algebraic equations in the unknowns  $\hat{u}$  and  $\hat{d}$  that can be expressed in the  
 578 following matrix form:

$$\begin{bmatrix} i\lambda + a_1 & a_2 \\ i\lambda(1 - a_4) & i\lambda(1 - a_5) + \pi^2/4 a_6 + \Omega - i\omega \end{bmatrix} \times \begin{bmatrix} \hat{u} \\ \hat{d} \end{bmatrix} = \begin{bmatrix} 0 \\ 0 \end{bmatrix}, \quad (\text{A.9})$$

579 while the “a” coefficients are defined as in *Camporeale et al.* [2007], namely:

$$a_1 = 2\beta/c_0^2, \quad a_2 = -(1 + 2c_D)\beta/c_0^2, \quad a_4 = 2\Phi_T, \quad a_5 = -2c_D\Phi_T, \quad a_6 = \frac{r}{\beta\sqrt{\theta_0}}. \quad (\text{A.10})$$

580 A non-trivial solution of the linear system A.9 exists when the determinant of the  
 581 matrix of coefficients vanishes, which gives:

$$\Omega - i\omega = -i\lambda(1 - a_5) - \frac{\pi^2}{4}a_6 + a_2(1 - a_4)\frac{i\lambda}{a_1 + i\lambda}, \quad (\text{A.11})$$

582 whose real part reads:

$$\Omega = -\frac{\pi^2}{4}a_6 + a_2(1 - a_4)\frac{\lambda^2}{a_1^2 + \lambda^2}, \quad (\text{A.12})$$

583 which, substituting the coefficients (A.10), provides an expression for the bar growth  
 584 rate  $\Omega$ , namely:

$$\Omega = -\frac{\pi^2}{4}\frac{r}{\beta\sqrt{\theta_0}} + (1 + 2c_D)\frac{\beta}{c_0^2}(2\Phi_T - 1)\frac{\lambda^2}{4\beta^2/c_0^4 + \lambda^2}. \quad (\text{A.13})$$

585 Marginal stability conditions are found by setting zero growth rate ( $\Omega = 0$ ) in Equation  
 586 (A.13), which gives:

$$\frac{4\beta_C^2}{c_0^2} \left[ \frac{\xi(\theta_0)}{r} (1 + 2c_D) - \frac{1}{c_0^2\lambda^2} \right] = 0, \quad \xi(\theta_0) := \frac{\sqrt{\theta_0}}{\pi^2} (2\Phi_T - 1), \quad (\text{A.14a, b})$$

587 from which it is easy to derive an explicit expression for the critical aspect ratio  $\beta_C$ .

## 588 **Appendix B Critical aspect ratio according to empirical free bars pre-** 589 **dictors**

590 In this section, we re-express existing empirical criteria in terms of the critical  
 591 width-to-depth ratio, as needed for a direct comparison with our formula (7).

### 592 **The criterion of *Muramoto and Fujita* [1978]**

593 This criterion for the formation of free alternate bars can be expressed as [see  
 594 *Jaeggi*, 1984]:

$$\frac{D_0/d}{(W/d)^{0.67}} < 0.45, \quad (\text{B.1})$$

595 Once expressed in terms of the channel aspect ratio, Equation (B.1) reads:

$$\beta > \beta_C = \frac{1}{2} 0.45^{-1/0.67} \left( \frac{D_0}{d} \right)^{1/0.67-1} = 1.647 \left( \frac{D_0}{d} \right)^{0.493}, \quad (\text{B.2})$$

596 which depends on the relative submergence  $D_0/d$  as illustrated in Figure B.1.

### 597 **The criterion of Jaeggi [1984]**

598 The bar formation criterion provided Jaeggi [1984] (see their Equation (8)), ex-  
599 pressed by means of our notation, reads:

$$\frac{\theta}{\theta_i} < 2.93 \log \left( \frac{\theta}{\theta_i} \frac{W}{D} \right) - 3.13 \left( \frac{W}{d} \right)^{0.15}, \quad (\text{B.3})$$

600 which can be also rewritten in terms of the channel aspect ratio  $\beta$  as:

$$2.93 \log \left( \frac{\theta}{\theta_i} 2\beta \right) - 3.13 \left( \frac{D_0}{d} 2\beta \right)^{0.15} - \frac{\theta}{\theta_i} > 0. \quad (\text{B.4})$$

601 Despite not allowing for deriving an explicit expression, Equation B.7 can be numeri-  
602 cally solved to obtain the critical aspect ratio  $\beta_C$ .

603 However, it is worth highlighting that a critical aspect ratio does not always exist.  
604 This can be noticed by analyzing the left hand side of the inequality (B.7), which does  
605 not increase monotonically with  $\beta$  but it shows a maximum when:

$$\beta = k \frac{d}{D_0}, \quad k = \frac{1}{2} \left( \frac{2.93}{3.13 \cdot 0.15} \right)^{1/0.15} = 1.00 \cdot 10^5. \quad (\text{B.5})$$

606 A critical value of the aspect ratio exists only if the maximum value is positive, as  
607 given by substituting (B.5) into (B.7):

$$2.93 \log \left( \frac{\theta}{\theta_i} 2k \frac{d}{D_0} \right) - \frac{2.93}{0.15} - \frac{\theta}{\theta_i} > 0, \quad (\text{B.6})$$

608 which can be expressed in terms of the relative submergence as follows:

$$\frac{D_0}{d} < \frac{\theta}{\theta_i} k_2 \exp \left( -\frac{1}{2.93} \frac{\theta}{\theta_i} \right), \quad k_2 = 2k \exp \left( -\frac{1}{0.15} \right) = 254.5. \quad (\text{B.7})$$

609 For Shields numbers in the range 1–6 times  $\theta_i$ , as usually the case of gravel bed rivers at  
610 bankfull conditions [Parker *et al.*, 2007], Equation (B.7) gives minimum values of  $D_0/d$   
611 between 181 and 274. For higher relative submergence  $D/d$ , Equation (B.3) is never  
612 satisfied, which implies that bars are not expected to form regardless of the value of  $\beta$   
613 (see Figure B.1). It is worth noticing, however, that this prediction seems essentially  
614 a mathematical artifact, as the empirical formula was derived from observations in  
615 conditions of relatively low submergence ( $D_0/d < 30$ ).

### 616 **The criterion of Yalin and Da Silva [2001]**

617 This criterion is based on the empirical definition of a threshold value of the chan-  
618 nel aspect ratio that only depends on the relative submergence ( $D_0/d$ ). Specifically,  
619 it can be expressed by means on the following piecewise-linear function:

$$\beta_C = \begin{cases} \frac{1}{8} \frac{D_0}{d} & \text{if } \frac{D_0}{d} < 100 \\ 12.5 & \text{if } \frac{D_0}{d} \geq 100 \end{cases}. \quad (\text{B.8})$$

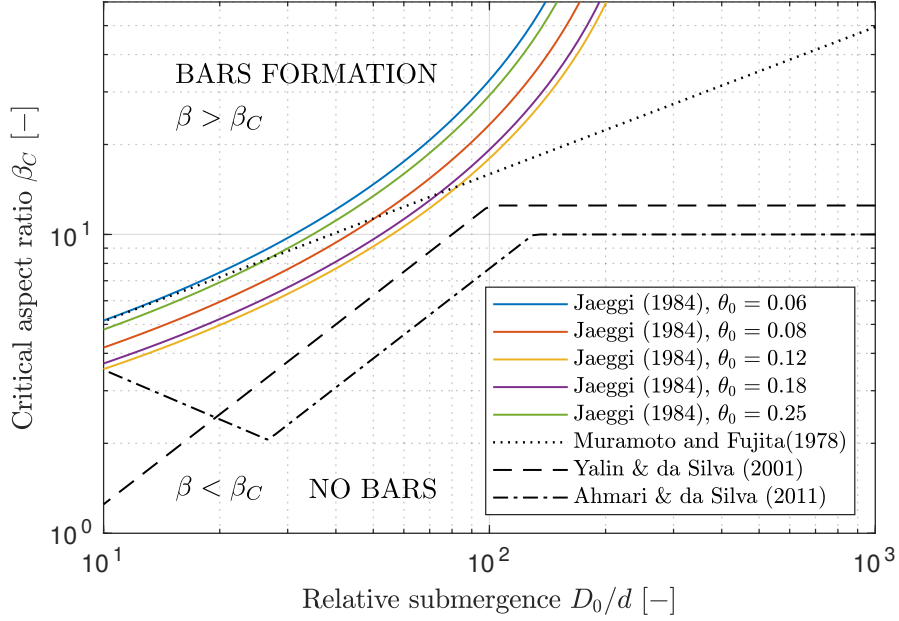


Figure B.1: Critical aspect ratio for the formation of free migrating bars according to the empirical criteria of *Muramoto and Fujita* [1978] (dotted line), *Jaeggi* [1984] (solid lines, depending on the Shields number  $\theta_0$ ), *Yalin and Da Silva* [2001] (dashed line) and [*Ahmari and Da Silva*, 2011] (dashed-dotted line). For all the criteria, bars are expected to form when the width-to-depth ratio exceeds the critical threshold.

620 **The criterion of *Ahmari and Da Silva* [2011]**

621 This criterion can be regarded as an updated version of *Yalin and Da Silva*  
 622 [2001], where the constant aspect ratio for high values of  $D_0/d$  is slightly reduced,  
 623 and where a third branch of the solution is introduced to consider a decrease of the  
 624 critical width-to-depth ratio for small values of the relative submergence. Specifically,  
 625 the authors proposed the following piecewise-linear function:

$$\beta_C = \begin{cases} 12.5 \left(\frac{D_0}{d}\right)^{-0.55} & \text{if } \frac{D_0}{d} < 26.69 \\ \frac{1}{13} \frac{D_0}{d} & \text{if } 26.69 \leq \frac{D_0}{d} < 130 \\ 10 & \text{if } \frac{D_0}{d} \geq 130 \end{cases} \quad (\text{B.9})$$

626 A comparison among the different expressions is illustrated in Figure B.1.

627 **Acknowledgments**

628 All experimental data are available at [https://bitbucket.org/Marco\\_Redolfi/](https://bitbucket.org/Marco_Redolfi/free_bars_analysis)  
 629 [free\\_bars\\_analysis](https://bitbucket.org/Marco_Redolfi/free_bars_analysis). I thank prof. Marco Tubino and prof. Walter Bertoldi for  
 630 kindly providing data they previously collected and organized.

631 **References**

- 632 Adami, L., W. Bertoldi, and G. Zolezzi (2016), Multidecadal dynamics of alternate  
 633 bars in the Alpine Rhine River, *Water Resources Research*, *52*, 8938–8955, doi:10.  
 634 1002/2015WR018228.
- 635 Ahmari, H., and A. M. F. Da Silva (2011), Regions of bars, meandering and braiding  
 636 in da Silva and Yalin’s plan, *Journal of Hydraulic Research*, *49*(6), 718–727, doi:  
 637 10.1080/00221686.2011.614518.
- 638 Ashida, K., and Y. Shiomi (1966), Study on the hydraulics behaviour of meander in  
 639 channels, *Disaster Prevention Research Institute Annuals*, pp. 457–477.
- 640 Baar, A. W., J. de Smit, W. S. J. Uijttewaal, and M. G. Kleinhans (2018), Sed-  
 641 iment Transport of Fine Sand to Fine Gravel on Transverse Bed Slopes in Ro-  
 642 tating Annular Flume Experiments, *Water Resources Research*, *54*(1), 19–45, doi:  
 643 10.1002/2017WR020604.
- 644 Bertagni, M. B., and C. Camporeale (2018), Finite amplitude of free alternate  
 645 bars with suspended load, *Water Resources Research*, *54*, 9759–9773, doi:10.1029/  
 646 2018WR022819.
- 647 Bertagni, M. B., P. Perona, and C. Camporeale (2018), Parametric transitions be-  
 648 tween bare and vegetated states in water-driven patterns, *Proceedings of the Na-  
 649 tional Academy of Sciences*, *115*(32), 8125–8130, doi:10.1073/pnas.1721765115.
- 650 Blondeaux, P., and G. Seminara (1985), A Unified Bar Bend Theory of River Meanders,  
 651 *Journal of Fluid Mechanics*, *157*, 449–470.
- 652 Callander, R. A. (1969), Instability and river channels, *Journal of Fluid Mechanics*,  
 653 *36*(3), 465–480, doi:10.1017/S0022112069001765.
- 654 Camporeale, C., P. Perona, A. Porporato, and L. Ridolfi (2007), Hierarchy of models  
 655 for meandering rivers and related morphodynamic processes, *Reviews of Geophysics*,  
 656 *45*(1), 1–28, doi:10.1029/2005RG000185.
- 657 Caponi, F., A. Koch, W. Bertoldi, D. F. Vetsch, and A. Siviglia (2019), When  
 658 Does Vegetation Establish on Gravel Bars? Observations and Modeling in the  
 659 Alpine Rhine River, *Frontiers in Environmental Science*, *7*(August), 1–18, doi:  
 660 10.3389/fenvs.2019.00124.
- 661 Carlin, M., M. Redolfi, and M. Tubino (2021), The long-term response of alternate  
 662 bars to the hydrological regime, *Water Resour. Res.*, *Submitted*.
- 663 Chang, H.-Y., D. B. Simons, and D. A. Woolhiser (1971), Flume experiments on  
 664 alternate bar formation, *Journal of Surveying and Mapping Division*.
- 665 Church, M., and S. P. Rice (2009), Form and growth of bars in a wandering gravel-bed  
 666 river, *Earth Surface Processes and Landforms*, *34*(10), 1422–1432, doi:10.1002/esp.  
 667 1831.
- 668 Claude, N., S. Rodrigues, V. Bustillo, J.-G. Br  h  ret, P. Tassi, and P. Jug   (2014),  
 669 Interactions between flow structure and morphodynamic of bars in a channel expan-  
 670 sion/contraction, Loire River, France, *Water Resources Research*, *50*(4), 2850–2873,  
 671 doi:10.1002/2013WR015182.
- 672 Colombini, M., and A. Stocchino (2012), Three-dimensional river bed forms, *J. Fluid  
 673 Mech*, *695*, 63–80, doi:10.1017/jfm.2011.556.
- 674 Colombini, M., G. Seminara, and M. Tubino (1987), Finite-amplitude alternate bars,  
 675 *Journal of Fluid Mechanics*, *181*(HY9), 213–232, doi:10.1017/S0022112087002064.
- 676 Cordier, F., P. Tassi, N. Claude, A. Crosato, S. Rodrigues, and D. Pham Van  
 677 Bang (2019), Numerical Study of Alternate Bars in Alluvial Channels With

- 678 Nonuniform Sediment, *Water Resources Research*, 55(4), 2976–3003, doi:10.1029/  
679 2017WR022420.
- 680 Crank, J. (1975), The mathematics of diffusion, *Oxford university press*, doi:10.1088/  
681 0031-9112/26/11/044.
- 682 Crosato, A., and E. Mosselman (2009), Simple physics-based predictor for the number  
683 of river bars and the transition between meandering and braiding, *Water Resources*  
684 *Research*, 45(3), 1–14, doi:10.1029/2008WR007242.
- 685 Crosato, A., and E. Mosselman (2020), An Integrated Review of River Bars for En-  
686 gineering, Management and Transdisciplinary Research, *Water*, 12(2), 596, doi:  
687 10.3390/w12020596.
- 688 Crosato, A., E. Mosselman, F. Beidmariam Desta, and W. S. J. Uijttewaai (2011),  
689 Experimental and numerical evidence for intrinsic nonmigrating bars in alluvial  
690 channels, *Water Resources Research*, 47(3), W03,511, doi:10.1029/2010WR009714.
- 691 Crosato, A., F. B. Desta, J. Cornelisse, F. Schuurman, and W. S. J. Uijttewaai  
692 (2012), Experimental and numerical findings on the long-term evolution of mi-  
693 grating alternate bars in alluvial channels, *Water Resources Research*, 48(6), doi:  
694 10.1029/2011WR011320.
- 695 Duró, G., A. Crosato, and P. Tassi (2016), Numerical study on river bar response to  
696 spatial variations of channel width, *Advances in Water Resources*, 93, 21–38, doi:  
697 10.1016/j.advwatres.2015.10.003.
- 698 Einstein, H. A., and H. W. Shen (1964), A study on meandering in straight al-  
699 luvial channels, *Journal of Geophysical Research*, 69(24), 5239–5247, doi:10.1029/  
700 jz069i024p05239.
- 701 Engelund, F. (1981), The motion of sediment particles on an inclined bed, *Progress*  
702 *Rep*, 53.
- 703 Engelund, F., and E. Hansen (1967), A monograph on sediment transport in alluvial  
704 streams, *Technical University of Denmark Ostervoldgade 10, Copenhagen K*.
- 705 Federici, B., and G. Seminara (2006), Effect of suspended load on sandbar instability,  
706 *Water Resources Research*, 42(7), 1–11, doi:10.1029/2005WR004399.
- 707 Ferguson, R. I., D. J. Bloomer, and M. Church (2011), Evolution of an advancing gravel  
708 front: Observations from Vedder Canal, British Columbia, *Earth Surface Processes*  
709 *and Landforms*, 36(9), 1172–1182, doi:10.1002/esp.2142.
- 710 Fredsoe, J. (1978), Meandering and Braiding of Rivers, *Journal of Fluid Mechanics*,  
711 84(November), 609–624, doi:10.1017/S0022112078000373.
- 712 Fujita, Y., and Y. Muramoto (1982), Experimental Study on Stream Channel Processes  
713 in Alluvial Rivers, *Tech. Rep. 288*.
- 714 García, M. H., and Y. Niño (1993), Dynamics of sediment bars in straight and mean-  
715 dering channels: experiments on the resonance phenomenon, *Tech. Rep. January*,  
716 doi:10.1080/00221689309498815.
- 717 Garcia Lugo, G. A., W. Bertoldi, A. J. Henshaw, and A. M. Gurnell (2015), The effect  
718 of lateral confinement on gravel bed river morphology, *Water Resources Research*,  
719 51(9), 7145–7158, doi:10.1002/2015WR017081.
- 720 Hall, P. (2004), Alternating bar instabilities in unsteady channel flows  
721 over erodible beds, *Journal of Fluid Mechanics*, 499(499), 49–73, doi:10.1017/  
722 S0022112003006219.
- 723 Ikeda, S. (1982), Prediction of alternate bar wavelength and height, *Saitama University*  
724 *Faculty of Engineering Construction Research Report*, (12), p23—45.
- 725 Ikeda, S. (1984), Prediction of Alternate Bar Wavelength and Height, *Journal of*  
726 *Hydraulic Engineering*, 110(4), 371–386, doi:10.1061/(ASCE)0733-9429(1984)110:  
727 4(371).
- 728 Jaballah, M., B. Camenen, L. Pénard, and A. Paquier (2015), Alternate bar develop-  
729 ment in an alpine river following engineering works, *Advances in Water Resources*,  
730 81, 103–113, doi:10.1016/j.advwatres.2015.03.003.

- 731 Jaeggi, M. N. R. (1984), Formation and Effects of Alternate Bars, *Journal of Hydraulic*  
732 *Engineering*, 110(2), 142–156, doi:10.1061/(ASCE)0733-9429(1984)110:2(142).
- 733 Jäggi, M. (1983), Mitteilungen der Versuchsanstalt für Wasserbau , Alternierende  
734 Kiesbanke, (62).
- 735 Jourdain, C., N. Claude, P. Tassi, F. Cordier, and G. Antoine (2019), Morphodynamics  
736 of alternate bars in the presence of riparian vegetation, *Earth Surface Processes and*  
737 *Landforms*, 1122(February), 1100–1122, doi:10.1002/esp.4776.
- 738 Kinoshita, R. (1961), Investigation of channel deformation in Ishikari River, *Report of*  
739 *Bureau of Resources, Dept. Science and Technology, Japan*, 174.
- 740 Lanzoni, S. (2000), Experiments on bar formation in a straight flume: 1. Uniform sed-  
741 iment, *Water Resources Research*, 36(11), 3337–3349, doi:10.1029/2000WR900160.
- 742 Lanzoni, S., and M. Tubino (1999), Grain sorting and bar instability, *Journal of Fluid*  
743 *Mechanics*, 393, 149–174, doi:10.1017/S0022112099005583.
- 744 Meyer-Peter, E., and R. Muller (1948), Formulas for bed load transport, *Proceedings of*  
745 *the 2nd congress of the International Association for Hydraulic Research*, 2, 39–64.
- 746 Muramoto, Y., and Y. Fujita (1978), The classification of meso-scale river bed configu-  
747 ration and the criterion of its formation, in *Proceedings of the Japanese Conference*  
748 *on Hydraulics*, vol. 22, pp. 275–282, Japan Society of Civil Engineers.
- 749 Nelson, J. M. (1990), The initial instability and finite-amplitude stability of al-  
750 ternate bars in straight channels, *Earth Science Reviews*, 29(1-4), 97–115, doi:  
751 10.1016/0012-8252(0)90030-Y.
- 752 Nelson, P. A., and J. A. Morgan (2018), Flume experiments on flow and sediment  
753 supply controls on gravel bedform dynamics, *Geomorphology*, 323, 98–105, doi:10.  
754 1016/j.geomorph.2018.09.011.
- 755 Paola, C. (2000), Quantitative models of sedimentary basin filling, *Sedimentology*, 47,  
756 121–178, doi:10.1046/j.1365-3091.2000.00006.x.
- 757 Parker, G. (1976), On the cause and characteristic scales of meandering and braiding  
758 in rivers, *Journal of Fluid Mechanics*, 76(3), 457, doi:10.1017/S0022112076000748.
- 759 Parker, G. (1978), Self-formed straight rivers with equilibrium banks and mobile bed.  
760 Part 2. The gravel river, *Journal of Fluid Mechanics*, 89(01), 127–146, doi:10.1017/  
761 S0022112078002505.
- 762 Parker, G. (1990), Surface-based bedload transport relation for gravel rivers, *Journal*  
763 *of Hydraulic Research*, 28(4), 417–436, doi:10.1080/00221689009499058.
- 764 Parker, G., P. R. Wilcock, C. Paola, W. E. Dietrich, and J. Pitlick (2007), Physical  
765 basis for quasi-universal relations describing bankfull hydraulic geometry of single-  
766 thread gravel bed rivers, *Journal of Geophysical Research: Earth Surface*, 112(4),  
767 1–21, doi:10.1029/2006JF000549.
- 768 Qian, H., Z. Cao, H. Liu, and G. Pender (2017), Numerical modelling of alternate bar  
769 formation, development and sediment sorting in straight channels, *Earth Surface*  
770 *Processes and Landforms*, 42(4), 555–574, doi:10.1002/esp.3988.
- 771 Ragno, N., M. Redolfi, and M. Tubino (2021), Coupled Morphodynamics of River  
772 Bifurcations and Confluences, *Water Resources Research*, 57(1), 1–26, doi:10.1029/  
773 2020WR028515.
- 774 Redolfi, M., and M. Tubino (2014), A diffusive 1D model for the evolution of a braided  
775 network subject to varying sediment supply, in *River Flow 2014*, pp. 1153–1161, doi:  
776 10.1201/b17133-155.
- 777 Redolfi, M., G. Zolezzi, and M. Tubino (2016), Free instability of channel bifurcations  
778 and morphodynamic influence, *Journal of Fluid Mechanics*, 799, 476–504, doi:10.  
779 1017/jfm.2016.389.
- 780 Redolfi, M., M. Welber, M. Carlin, M. Tubino, and W. Bertoldi (2020), Morphometric  
781 properties of alternate bars and water discharge: a laboratory investigation, *Earth*  
782 *Surface Dynamics*, 8(3), 789–808, doi:10.5194/esurf-8-789-2020.
- 783 Repetto, R., M. Tubino, and C. Paola (2002), Planimetric instability of chan-  
784 nels with variable width, *Journal of Fluid Mechanics*, 457, 79–109, doi:10.1017/

- 785 S0022112001007595.
- 786 Rodrigues, S., E. Mosselman, N. Claude, C. L. Wintenberger, and P. Juge (2015),  
787 Alternate bars in a sandy gravel bed river: Generation, migration and interactions  
788 with superimposed dunes, *Earth Surface Processes and Landforms*, *40*(5), 610–628,  
789 doi:10.1002/esp.3657.
- 790 Seminara, G. (2010), Fluvial Sedimentary Patterns, *Annual Review of Fluid Mechan-*  
791 *ics*, *42*(1), 43–66, doi:10.1146/annurev-fluid-121108-145612.
- 792 Seminara, G., and M. Bolla Pittaluga (2012), Reductionist versus holistic approaches  
793 to the study of river meandering: An ideal dialogue, *Geomorphology*, *163-164*, 110–  
794 117, doi:10.1016/j.geomorph.2011.06.037.
- 795 Serlet, A. J., A. M. Gurnell, G. Zolezzi, G. Wharton, P. Belleudy, and C. Jour-  
796 dain (2018), Biomorphodynamics of alternate bars in a channelized, regulated river:  
797 An integrated historical and modelling analysis, *Earth Surface Processes and Land-*  
798 *forms*, *43*(9), 1739–1756, doi:10.1002/esp.4349.
- 799 Shaw, J. B., and B. McElroy (2016), Backwater number scaling of alluvial bed  
800 forms, *Journal of Geophysical Research: Earth Surface*, *121*, 1436–1455, doi:10.  
801 1002/2016JF003861.
- 802 Siviglia, A., G. Stecca, D. Vanzo, G. Zolezzi, E. F. Toro, and M. Tubino (2013), Nu-  
803 merical modelling of two-dimensional morphodynamics with applications to river  
804 bars and bifurcations, *Advances in Water Resources*, *52*, 243–260, doi:10.1016/j.  
805 advwatres.2012.11.010.
- 806 Struiksma, N., K. W. Olesen, C. Flokstra, and H. J. De Vriend (1985), Bed deformation  
807 in curved alluvial channels, *Journal of Hydraulic Research*, *23*(1), 57–79, doi:10.  
808 1080/00221688509499377.
- 809 Sukegawa, N. (1971), Study on meandering of streams in straight channels, *Report of*  
810 *Bureau of Resources, Dept. Science and Technology, Japan*, pp. 335–363.
- 811 Tharwat, A. (2018), Classification assessment methods, *Applied Computing and In-*  
812 *formatics*, *17*(1), 168–192, doi:10.1016/j.aci.2018.08.003.
- 813 Tubino, M. (1991), Growth of alternate bars in unsteady flow, *Water Resources Re-*  
814 *search*, *27*(1), 37–52, doi:10.1029/90WR01699.
- 815 Tubino, M., and G. Seminara (1990), Free–forced interactions in developing meanders  
816 and suppression of free bars, *Journal of Fluid Mechanics*, *214*(4), 131–159, doi:10.  
817 1017/S0022112090000088.
- 818 Tubino, M., R. Repetto, and G. Zolezzi (1999), Free bars in rivers, *Journal of Hy-*  
819 *draulic Research*, *37*(6), 759–775, doi:10.1080/00221689909498510.
- 820 Wilkinson, S. N., I. D. Rutherford, and R. J. Keller (2008), An experimental test of  
821 whether bar instability contributes to the formation, periodicity and maintenance  
822 of pool-riffle sequences, *Earth Surface Processes and Landforms*, *33*(11), 1742–1756,  
823 doi:10.1002/esp.1645.
- 824 Yalin, M. S., and A. M. F. Da Silva (2001), Fluvial processes, IAHR Delft, The  
825 Netherlands.